# Generating Arbitrary Chemical Patterns for Multi-Point Dosing of Single Cells.

**ARTICLE** *in* ANALYTICAL CHEMISTRY · FEBRUARY 2013

Impact Factor: 5.64 · DOI: 10.1021/ac4001089 · Source: PubMed



**3 AUTHORS**, INCLUDING:

Samira Moorjani
University of Washington Seattle
**6** PUBLICATIONS **212** CITATIONS

SEE PROFILE

analytical chemistry

Article

pubs.acs.org/ac

# Generating Arbitrary Chemical Patterns for Multipoint Dosing of Single Cells

Todd J. Hoppe, Samira G. Moorjani,[†] and Jason B. Shear*

Department of Chemistry and Biochemistry, The University of Texas at Austin, 1 University Station, A5300, Austin, Texas, 78712-0165, United States

Supporting Information

**ABSTRACT:** Living cells reside within anisotropic microenvironments that orchestrate a broad range of polarized responses through physical and chemical cues. To unravel how localized chemical signals influence complex behaviors, tools must be developed for establishing patterns of chemical gradients that vary over subcellular dimensions. Here, we present a strategy for addressing this critical need in which an arbitrary number of chemically distinct, subcellular dosing streams are created in real time within a microfluidic environment. In this approach, cells are cultured on a thin polymer membrane that serves as a barrier between the cell-culture environment and a reagent chamber containing multiple reagent species flowing in parallel under low Reynolds number conditions. Focal ablation of the membrane creates pores that allow solution to flow from desired regions within this reagent pattern into the cell-culture chamber, resulting in narrow, chemically distinct dosing streams. Unlike previous dosing strategies, this system provides the capacity to tailor arbitrary patterns of reagents on the fly to suit the geometry and orientation of specific cells.

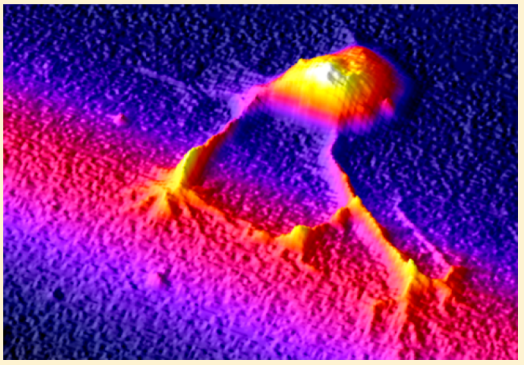

Cells in vivo function in a complex milieu of time-varying chemical gradients, signals that regulate processes from differentiation until cell death. In many circumstances, cells must integrate instructions from a host of cues that modulate activity in nonlinear and often conflicting fashion.[1−4] Neurons in the central nervous system, for example, can receive numerous excitatory and inhibitory inputs along their dendritic tree that contribute differentially to the firing status of the cell.[5] Migration of immune cells is orchestrated by a range of attractive and repulsive factors, including cytokines and foreign peptides, which act through gradients that may be simultaneously presented to the surface of a leukocyte or neutrophil.[6,7] Neurons also rely on coexisting gradients of attractive and repulsive factors, for both migration and axonal pathfinding.[8,9] Although there has been growing realization of the influence of microscopic chemical gradients on cellular behavior,[10] attempts to create complex distributions of cellular effectors have faced serious challenges.

To systematically assess effects from subcellular chemical signals, various strategies have been developed for creating chemical gradients on micrometer dimensions. Micropositioned puffer pipets are commonly used to expel subnanoliter volumes of effectors near a cell membrane;[11−13] however, physical constraints of micromanipulators limit both the number of simultaneous dosing sites and the speed at which a pipet can be repositioned to a new site of interest. Optical uncaging of caged effectors provides high-resolution chemical dosing without the mechanical limitations inherent to puffer pipets,[14,15] but is restricted to instances in which photocleavable dosing precursors can be synthesized. Whether introduced via pipet or by uncaging, diffusion of a dosing bolus from its initial delivery site yields a time-dependent gradient that often dissipates within milliseconds, preventing use of these approaches for characterizing cellular responses to sustained chemical gradients.

As an alternative, microfluidic architectures can be used to create defined laminar flow patterns within cellular microenvironments, a strategy that has been adopted for in vitro chemical dosing of cultured cells.[16−20] Whitesides and coworkers reported a platform in which confluent microfluidic streams in a poly(dimethylsiloxane) (PDMS) microchip could be used to form steep, stable gradients of cellular effectors, an approach that was exploited to direct chemotaxis of cultured cells over distances as small as several micrometers.[21,22] A major limitation of this approach is that the number, position, and orientation of desired gradients are constrained by the preset geometry of the microfabricated device and thus cannot be tailored to accommodate arbitrary geometries and arrangements that cultured cells adopt within the device.

To extend the capabilities of microfluidic systems for in vitro chemical dosing, we previously reported a stacked laminar-flow system in which a dosing reagent is separated from a cell-culture region by a thin polymer membrane that can be ablated at user-defined positions using the focused output of a pulsed laser.[23] Ablation pores serve as conduits for reagent entry into

**Received:** January 11, 2013
**Accepted:** February 20, 2013
**Published:** February 20, 2013

   dx.doi.org/10.1021/ac4001089 | *Anal. Chem.* 2013, 85, 3746−3751

the cell-culture environment, where laminar-flow conditions result in the formation of well-defined dosing streams that can extend for up to hundreds of micrometers with minimal diffusion. A given stream diameter depends on the size of a pore, the solution flow rate, and how far the stream has traveled from its inception at a pore. Optimization of these parameters allows targets to be dosed over regions as small as 10 $\mu$m.[23] In addition, by incorporating a means to rotate flow directionality within the cell-culture region, it is possible to reorient dosing streams and, hence, chemical gradients with millisecond resolution.[24]

A defining limitation of this membrane-based approach has been its reliance on a single reservoir to supply all pores with the same dosing reagent. Although this design principle provides great flexibility for multisite dosing, many applications require the ability to dose cells with different reagents at well-defined subcellular positions. Use of multiple reagents, for example, would enable studies aimed at quantifying proximity effects of multiple synergistic or competing cues for processes such as membrane depolarization and chemotaxis and for tracking redistribution of subcellular organelle populations (e.g., vesicle pools).

Here, we report a strategy for generating multiple reagent streams within cell-culture environments that can deliver distinct dosing species to different, targeted subcellular regions. This approach can be used to maintain steep, stable gradients for hours or longer or, alternatively, can produce streams whose qualitative or quantitative composition can be modified on subsecond time scales.

## RESULTS AND DISCUSSION

**Chip Design.** To implement this concept, a reagent flow cell comprised of multiple variable-flow-rate inlets and a single outlet is stacked with a cell-culture chamber flowing at 90° to the reagent chamber. A 7.6 $\mu$m thick polyimide membrane serves as a barrier between the two flow cells, providing a biocompatible surface for cell culture[25,26] and an efficient substrate for ablating low-micrometer-diameter pores using a tightly focused pulsed (Nd:YAG) laser beam (Figures S-1 and S-2, Supporting Information). A pressure gradient between the two flow cells forces reagents through pores into the cell-culture chamber, where they become entrained by laminar flow into narrow streams that are directed at downstream subcellular targets.

Relatively rapid, laminar flow in the reagent flow cell limits mixing across boundaries separating confluent reagents. As a consequence, distinct reagent "reservoirs" are established that are individually sampled by focal ablation of pores to create dosing streams of distinct composition.

**Reagent Switching and Variable Concentration Control.** The boundary position between confluent, laminar streams in a rigid flow channel is dictated by the relative volumetric flow rates,[27] a characteristic we exploit here to alter, in real time, which species in the reagent flow cell is positioned beneath specific pores in the polyimide membrane. For example, if the flow rate of one reagent is increased relative to that of a second reagent, the boundary will encroach on the latter reagent. Hence, as the boundary passes beneath a pore, the solution traveling through the pore into the cell culture chamber will also change in composition. This phenomenon is depicted schematically (Figure 1a) and experimentally using a confluent system of fluorescein and nonfluorescent HEPES-buffered saline (HBS) in the reagent flow cell (Figure 1b).

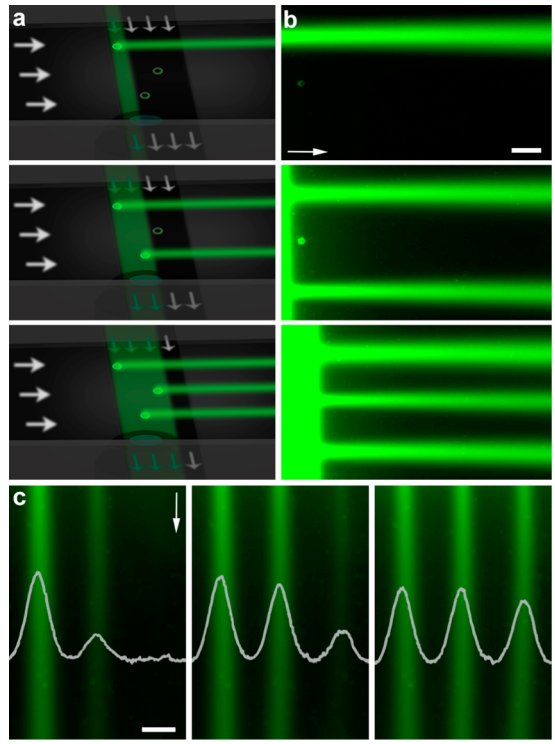


**Figure 1.** Production of dosing streams using a confluent reagent flow cell. (a) Schematic depicting use of a moving reagent boundary to initiate (or terminate) dosing from a set of staggered pores. Because flow in the dosing chamber is orthogonal to that in the reagent chamber, the horizontal position at which a pore is ablated dictates the order in which reagent flow is initiated (i.e., top, bottom, middle). (b) Implementation of the concept shown in (a) using confluent inlets of (50 $\mu$M) fluorescein and HBS buffer to feed a reagent flow cell. As the flow rate from the fluorescein inlet is increased, the boundary moves left to right in the image and fluorescein replaces HBS in the dosing streams. (c) Placement of pores at different positions relative to a diffuse fluorescein–HBS buffer boundary produces dosing streams of differing compositions. By moving a horizontal reagent boundary "downward" toward the field of view, the fluorescein concentration in three streams can be changed at different times. The plots show fluorescence (arbitrary units) as a function of distance across the image at points ~100 $\mu$m above the bottom of the image. Scale bars represent 50 $\mu$m.

Initially, fluorescein supplies the "top" pore (positioned to the left of the imaged area), with HBS overlapping the middle and lowest pores, yielding a single fluorescein dosing stream across the top of the image (Figure 1a,b, top panels). By increasing the supply rate of fluorescein to the reagent flow cell, the boundary between fluorescein and HBS shifts rightward, first passing a pore positioned near the bottom left in the image (Figure 1a,b, middle panels) and finally the rightmost pore positioned near the vertical center of the image (Figure 1a,b, lower panels). In this manner, reagent streams can be reversibly introduced to the cell-culture chamber at desired positions and times, with temporal ordering dictated by the horizontal arrangement of pores.

This proof-of-concept experiment demonstrates the ability to supply distinct components to different pores using two visually distinct reagents, a nonfluorescent buffer and a dye; however, the only fundamental limitation on stream composition is that reagents must be soluble in the solvent system(s) that are employed. It should be possible, for example, to investigate


dx.doi.org/10.1021/ac4001089 | Anal. Chem. 2013, 85, 3746–3751

neuronal signal integration by targeting streams of excitatory and inhibitory ligands to defined sites on a neuronal process and to dynamically substitute one type of input for the other.

These results illustrate a key design consideration in this microfluidic platform: by establishing flow in the two channels along axes orthogonal to each other, the position and composition of dosing streams can be controlled independently of one another. In this way, placement of a pore along the axis normal to solution flow in the dosing chamber determines the location of a resultant stream while placement normal to solution flow in the reagent chamber (relative to the reagent boundary) dictates stream content. Were flows in the two channels set parallel to each other, it would not be possible to interdigitate streams of differing composition (Figure 1b, middle panel).

Lateral diffusion at the boundary of two confluent laminar streams yields a narrow region of continuously variable reagent concentration which can be expanded by slowing the flow rate within the reagent chamber (Figure S-3, Supporting Information). By controlling the position of this more diffuse interfacial region such that it overlaps pores, it is possible to create dosing streams consisting of any ratio of two reagents supplied separately in the two confluent streams or to tune the concentration of a single reagent at the boundary of confluent buffer (Figure 1c; Figure S-4, Supporting Information).

**Subcellular Targeting with Multiple Reagents.** This high-resolution dosing strategy can be extended to generate complex reagent patterns composed of multiple reagents. In Figure 2, a reagent flow cell fed by five confluent streams is used to produce dosing streams containing 4′,6-diamidino-2-phenylindole (DAPI; blue, 1), rhodamine B (red, 2), and fluorescein (green, 3). The upper left panel shows a false-color composite image of the reagent flow cell, with rectangular regions of interest demonstrating where three dosing streams are subsequently produced by pore ablation within the distinct reagent environments (upper right). By creating a set of pores at appropriate coordinates relative to the reagent reservoir (lower left), this configuration can be used to generate dosing maps of any arbitrary sequence (lower right).

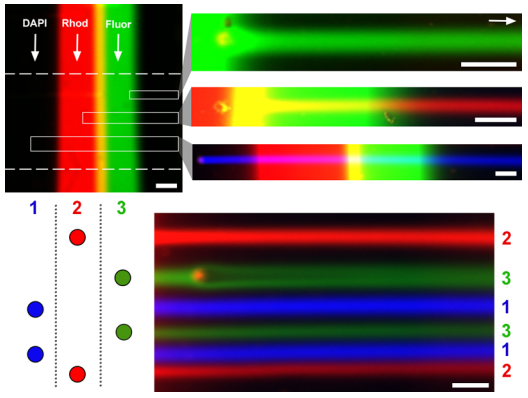


**Figure 2.** Generation of arbitrary multireagent dosing maps. Upper left: In a five-inlet reagent flow cell, laminar flow streams of (left to right) HBS buffer, 250 $\mu$M DAPI, 25 $\mu$M rhodamine B, 25 $\mu$M fluorescein, and HBS buffer flow in parallel from top to bottom. This flow cell is separated from a cell-culture flow cell flowing left to right by a thin polyimide membrane. Because of filtering effects of the membrane, DAPI fluorescence cannot be observed in the reagent flow cell. Upper right: Dosing streams composed of fluorescein (top), rhodamine B (middle), and DAPI (bottom) produced by the multireagent flow cell. Bottom: By patterning the pores in a user-designed arrangement, any conceivable pattern of interdigitated streams can be produced for downstream dosing. For example, the arrangement of pores shown in the lower left panel produces the pattern of streams shown in the lower right image. The uppermost green stream can be seen passing over and splitting around a surface feature on the membrane. Concentration variability in red streams results from pore occlusion/incomplete ablation. The scale bar in the upper left image represents 100 $\mu$m. All other scale bars represent 50 $\mu$m.

To evaluate applicability of this strategy for multicomponent targeting of subcellular domains, a reagent flow cell was constructed using three confluent inlets (two reagents and a buffer line), a configuration that can be used to initiate and terminate dosing at desired times by overlapping the buffer region with a given pore. As a proof of concept for subcellular dosing, individual cells were dosed at two distinct sites with membrane-permeant reagents that display low intrinsic fluorescence outside the cytosol. Figure 3a demonstrates the result of dosing a neuronally differentiated mouse neuroblastoma–rat glioma hybrid (NG108-15) cell with two cellular trackers—MitoTracker Red CMXRos and SYTO 13 green fluorescent stain—at the soma and on a neuritic process, respectively, for a period of 1 min. This procedure results in selective labeling of these subcellular domains (fluorescence intensity surface plot, Figure 3b). Although a small amount of green fluorescence is measured in the soma, normalization of signal based on dosing studies performed using a uniform bath

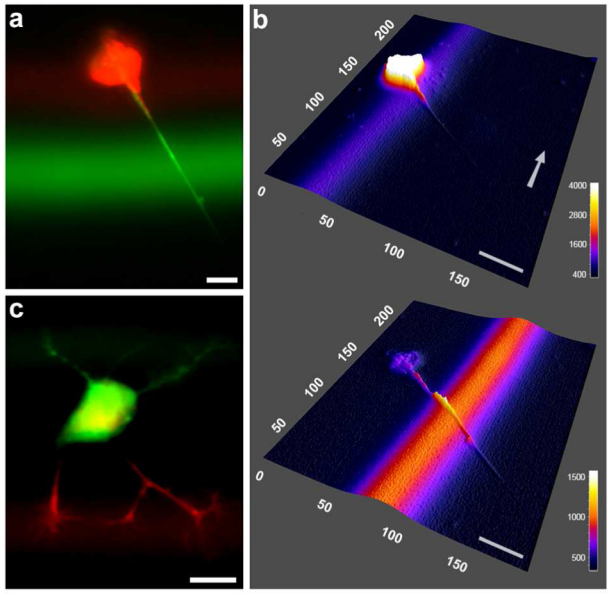


**Figure 3.** Subcellular labeling with multiple dyes. (a) A single NG108-15 cell is simultaneously dosed near the soma by a stream of 1 $\mu$M MitoTracker Red CMXRos and at a neuritic process by a stream of 2.5 $\mu$M SYTO 13 green fluorescent stain. (b) Separate red (top) and green (bottom) fluorescence channels from (a) depicted as fluoresecence intensity surface plots. Green fluorescence (SYTO) at the soma relative to its neuritic process is more than 40-fold below the levels seen in control experiments. Red fluorescence (MitoTracker) at the soma is saturated at the exposure time required for visualizing low-level staining in the neurite. (c) A single NG108-15 cell is dosed on opposing neuritic arborizations using 1 $\mu$M MitoTracker Green FM (top) and 1 $\mu$M MitoTracker Red CMXRos (bottom). Reagents contain 10 $\mu$M fluorescein and 10 $\mu$M rhodamine B, respectively, to aid visualization of the streams. Scale bars represent 20 $\mu$m.


dx.doi.org/10.1021/ac4001089 | Anal. Chem. 2013, 85, 3746–3751

of SYTO 13 indicates that dye localization in the neurite is enhanced using targeted dosing by at least 40-fold. In a similar study, selective dosing of opposing NG108-15 arborizations is achieved using MitoTracker Green FM and MitoTracker Red CMXRos (Figure 3c). At the relatively high concentrations used in this study (1−2.5 $\mu$M concentration of each reagent), appearance of all dyes is observed in the cytosol as the dye accumulates over time. This approach can be used to assess the dynamics of dye redistribution within cells after focal entry (Figure S-5, Supporting Information).

The versatile dosing strategy described here provides a means to define extracellular chemical environments with high spatiotemporal resolution, opening opportunities for assessing how cells integrate instructions from a host of cues that modulate activity. Unlike previous methods,[26−31] this approach enables the extracellular medium to be tailored at many sites in parallel with no necessary relationship between the cellular position and the content of the extracellular dosing solution. This key development opens the possibility, for example, to dose alternating segments of a neurite with an agonist and antagonist or to expose cells to arbitrarily defined step gradients of essentially any effector.

Although dosing in this unconstrained fashion is most readily performed when the reagent and cell-culture chambers support orthogonal flow, the independence of dosing composition and position can be maintained as long as flow in the two channels is not fully parallel. As a consequence, it also should be feasible to combine the multireagent dosing described in the current work with stream-steering capabilities achieved by introducing multidirectional flow within the cell-culture chamber.[24]

## EXPERIMENTAL SECTION

**Chip Design and Assembly.** The dosing system used in these studies (Figure S-1, Supporting Information) consists of two distinct flow cells separated by a 7.6 $\mu$m thick polyimide membrane (Kapton 30HN, DuPont). The dosing (cell-culture) flow chamber, obtained from Grace Bio-Laboratories (440889B), has dimensions of 32 mm (length) × 2.5 mm (width) × 0.12 mm (height) and is provided with an adhesive for affixing the chamber to a substrate to define the final boundary of the flow environment. The reagent flow chamber is fabricated from 0.12 mm thick sheets of Secure-Seal adhesive (Grace Bio-Laboratories, SA-S-1L) using a 60 W $CO_2$ laser cutter (Universal Laser Systems, X-660) to have multiple channels measuring 1.5 mm wide and 10 mm long converging to a confluent channel measuring 1.5 mm wide and 19 mm long. The adhesive is then attached to a polycarbonate coverslip that is drilled to have corresponding 2 mm diameter inlet ports leading to a single outlet at the respective ends of the flow cell. Inlet and outlet ports are mated to supply and drain tubes, respectively, via press-fit tubing connectors (Grace Bio-Laboratories, 460003). Flow is controlled using a pair of programmable digital syringe pumps (Stoelting 53130, Braintree Scientific BS-9000, and New Era NE-300/NE-1600) connected to flow-cell inlets through platinum-cured silicone tubing (Cole-Parmer, 95802-01). For all experiments, the reagent flow cell is situated above the polyimide membrane (Figure S-1 is inverted for visualization of dosing streams). In the case of cell-culture studies, cells are loaded with the stacked flow cells inverted to allow adequate adhesion to the membrane, before flipping the device into its normal orientation.

In the initial step of assembling the device, the polyimide membrane is stretched taut using an 8 cm diameter aluminum spring-tension hoop that provides approximately equal tension from all directions. The membrane is then attached via double-sided adhesive tape to a 6 cm × 6 cm plastic (poly(oxymethylene)) frame. To maintain tension, a second frame is attached to the opposite side of the membrane through a set of screws at each corner, creating a sandwich around the polyimide membrane that holds the membrane flat. At this point, the membrane is cleaned and sterilized using a swipe of 70% ethanol and a 15 min exposure to UV light in a cell-culture hood. Flow cells are then adhered to both sides of the polyimide membrane.

When cell-dosing studies are performed, one side of the membrane is soaked with 1.0 mg $mL^{-1}$ rat-tail collagen (BD Biosciences, 354249) in a 30% ethanol/70% water (v/v) mixture overnight by overfilling the fully constructed cell-culture flow cell chamber. After overnight exposure to collagen, this flow cell is then rinsed with Leibovitz (L-15) medium (HyClone, SH30525) and cells are deposited on the surface by overfilling the flow cell with a concentrated solution of cells in L-15 medium (see the section "Cell Culture and Chemicals"). The entire device is then placed on the microscope stage in a home-built incubation chamber set to maintain cell temperatures at 34−35 °C and ∼40% relative humidity. Attachment and general appearance of cells are monitored for ∼1 h, and then L-15 medium is gently flowed over the cells (0.01 mL $min^{-1}$, corresponding to an average linear flow velocity of 0.5 mm $s^{-1}$), which washes away remaining free-floating or loosely attached cells.

After the reagent flow cell is filled (typically at an initial rate of 0.1 mL $min^{-1}$ for each solution), pores are introduced into the polyimide membrane using a focused Q-switched laser beam and flow rates are adjusted to produce desired stream characteristics. For all studies, solution is delivered at 0.10 mL $min^{-1}$ within the cell-culture chamber. Total initial flow rates ranging from 0.20 to 0.60 mL $min^{-1}$ are used in the reagent flow cell, with the overall rate affecting both the pressure within the reagent channel (which must be sufficient to drive solution through pores into the cell-culture channel) and the width of reagent boundaries. In three-component reagent flow cells, the initial overall flow rate is 0.6 mL $min^{-1}$, with a constant HBS buffer flow rate of 0.3 mL $min^{-1}$. In five-component reagent flow cells, the initial overall flow rate is 1.0 mL $min^{-1}$. Individual flow rates of confluent reagents can be adjusted to move the lateral position of the boundary. In general, boundaries are moved by increasing the flow rate of a single reagent, a procedure that can increase the overall reagent flow rate from its initial value by as much as ∼25%.

**Laser Ablation.** Localized ablation of the polyimide membrane is achieved using a Q-switched frequency-doubled (532 nm) Nd:YAG laser (JDS Uniphase, NG-10320-110) that has an average power output of >25 mW, a pulse width of ∼600 ps, and a repetition rate of 7.65 kHz. The beam is expanded and collimated before being directed into the back aperture of a 40× objective (Olympus UPlanFl, 0.75 NA). To achieve the most reproducible ablation, we have found that it is preferable to produce a Gaussian focus by slightly underfilling this objective. This approach reduces the maximum intensity at the focal point but extends the ablation voxel along the optical axis to more effectively ablate pores through the entire 7.6 $\mu$m thick membrane. A half-wave plate/polarizer pair situated immedi-


dx.doi.org/10.1021/ac4001089 | Anal. Chem. 2013, 85, 3746−3751

ately after the laser is used to tune the average power of the beam before the objective back-aperture to 8−10 mW.

A pulsed Uniblitz UHS1 shutter (Vincent Associates, VMM-T1) controls exposure during ablation of a pore, delivering a train of 10 ms exposure periods (∼76 laser pulses) repeated 2−5 times with 50 ms delays between adjacent exposures. This exposure procedure typically is sufficient to efficiently ablate pores in the polyimide membrane while allowing time for heat to dissipate in solution between exposures. In addition, use of multiple exposure periods appears to help dislodge bubbles that may be formed during the first pulse and are stuck to the lip of the pore. Use of these parameters results in a successful pore (i.e., one that produces a consistent reagent stream) in approximately 70% of attempts. The average diameter of pores as determined by scanning electron microscopy (SEM) is 3.9 ± 0.9 $\mu$m ($n$ = 50). Full width at half-maximum stream diameters shown in Figures 1−3 ranged from ∼15 to 45 $\mu$m, depending primarily on the solution flow rate in the dosing cell and the distance of the stream from a pore.

**Cell Culture and Chemicals.** Neuroblastoma glioma (NG108-15) cells, originally purchased from the American Type Culture Collection, are stored at concentrations of ∼500 000 cells $mL^{-1}$ in liquid nitrogen until they are needed for culture. When thawed, cells are cultured in Dulbecco's modified Eagle's medium (DMEM; Corning Cellgro) supplemented with 10% (v/v) fetal bovine serum (HyClone, AVJ82746), 1% (v/v) penicillin/streptomycin (MP Biomedicals), and 1× HAT ($1 \times 10^{-4}$ hypoxanthine, $2 \times 10^{-7}$ aminopterin, $1.6 \times 10^{-4}$ thymidine; 50× HAT solution was purchased from MediaTech). Flasks are maintained at 37 °C in a 5% $CO_2$ atmosphere at 100% relative humidity with media replacement every 2 days, and cells are split to a new flask every 4−5 days (depending on confluence) for up to 40 total passages. For loading into the flow device, cells are passaged from a confluent flask by exposure to 1 mL of 1× trypsin−EDTA (MediaTech) for 2 min (quenched with 5 mL of DMEM). Cells are removed from the flask and centrifuged for 3 min at 1000 rpm. The supernatant is then removed and replaced with sufficient L-15 medium to produce a suspension of $\sim 10^5$ cells $mL^{-1}$. At a volume of 10 $\mu$L, this procedure delivers approximately $10^3$ cells to the flow chamber (corresponding to 12 cells $mm^{-2}$ when settled). The cell field for these experiments is approximately 3.75 $mm^2$.

MitoTracker Green FM (M7514) and MitoTracker Red CMXRos (M7512) were purchased from Molecular Probes (Eugene, OR). Fluorescein and rhodamine B for fluorescent stream imaging were purchased from Sigma-Aldrich (St. Louis, MO). HBS buffer is prepared from 140 mM NaCl, 5 mM KCl, 750 $\mu$M $Na_2HPO_4 \cdot 7H_2O$, 6 mM dextrose, and 25 mM HEPES at pH 7.1.

**Microscopy.** Both fluorescence and light transmission images were acquired on a Zeiss Axiovert 135 inverted microscope using either a 10× objective (Zeiss Fluar, 0.5 NA) or a 20× objective (Zeiss Plan-Neofluar, 0.5 NA) and a Hamamatsu Orca II charge-coupled device (CCD) camera (C4742-98) controlled by MetaMorph imaging software (Molecular Devices). Fluorescence images required the use of a Zeiss HBO 100 mercury arc lamp and a three-position fluorescence slider module equipped with both fluorescein isothiocyanate (FITC) and tetramethylrhodamine isothiocyanate (TRITC) filter sets to ease switching between fluorescence channels. Images were processed using MetaMorph and ImageJ.

## CONCLUSIONS

The approach described here, based on stacked laminar-flow reagent and cell-culture chambers, provides a means to define extracellular chemical environments with high spatiotemporal resolution. Unlike previous methods, this approach provides the possibility to define the extracellular medium at many sites in parallel with no necessary relationship between the cellular position and the content of the extracellular dosing solution. This key development opens the possibility, for example, to dose alternating segments of a neurite with an agonist and antagonist or to expose cells to arbitrarily defined step gradients of essentially any effector. Additional functionality may be achieved by pairing the technique with previously reported stream-steering capabilities[24] and valving by controlled pore occlusion.[23] Additionally, the laser ablation properties of bulk PDMS[32] and methods for fabricating ultrathin sheets from the material[33] suggest that an integrated device, including a polymer membrane, could be fabricated entirely from a single material.

## ASSOCIATED CONTENT

### Supporting Information

Additional information as noted in text. This material is available free of charge via the Internet at http://pubs.acs.org.

## AUTHOR INFORMATION

### Corresponding Author

*E-mail: jshear@cm.utexas.edu.

### Present Address

†S.G.M.: Department of Bioengineering, University of Washington, 1705 NE Pacific St., Seattle, WA 98195, United States.

### Notes

The authors declare no competing financial interest.

## ACKNOWLEDGMENTS

This work was supported by grants from the Robert A. Welch Foundation (F-1331), the Norman Hackerman Advanced Research Program of Texas (003658-0231-2009), and the National Institutes of Health (1R43MH085396-01 to Minotaur Technologies, LLC). We gratefully acknowledge experimental assistance from Tim Hooper and advice from Eric Ritschdorff. J.B.S. is a Fellow of the Institute for Cellular and Molecular Biology.

## REFERENCES

(1) Li Jeon, N.; Baskaran, H.; Dertinger, S. K. W.; Whitesides, G. M.; Van De Water, L.; Toner, M. *Nat. Biotechnol.* **2002**, *20*, 826−830.
(2) Raper, J.; Mason, C. *Cold Spring Harbor Perspect. Biol.* **2010**, *2*, 1−21.
(3) Bargmann, C. I.; Horvitz, H. R. *Neuron* **1991**, *7*, 729−742.
(4) Marin, O. *Development* **2003**, *130*, 1889−1901.
(5) Maldve, R. E.; Zhang, T. A.; Ferrani-Kile, K.; Schreiber, S. S.; Lippmann, M. J.; Snyder, G. L.; Fienberg, A. A.; Leslie, S. W.; Gonzales, R. A.; Morrisett, R. A. *Nat. Neurosci.* **2002**, *5*, 641−648.
(6) Foxman, E. F.; Kunkel, E. J.; Butcher, E. C. *J. Cell Biol.* **1999**, *147*, 577−588.
(7) Lin, F.; Nguyen, C. M.-C.; Wang, S.-J.; Saadi, W.; Gross, S. P.; Jeon, N. L. *Ann. Biomed. Eng.* **2005**, *33*, 475−482.
(8) Forbes, E. M.; Thompson, A. W.; Yuan, J.; Goodhill, G. J. *Neuron* **2012**, *74*, 490−503.
(9) Marin, O.; Valiente, M.; Ge, X.; Tsai, L.-H. *Cold Spring Harbor Perspect. Biol.* **2010**, *2*, 1−20.
(10) Keenan, T. M.; Folch, A. *Lab Chip* **2008**, *8*, 34−57.

(11) Prager, D. J.; Bowman, R. L.; Vurek, G. G. *Science* **1965**, *147*, 606−608.
(12) Stosiek, C. *Proc. Natl. Acad. Sci. U.S.A.* **2003**, *100*, 7319−7324.
(13) Ming, G.; Song, H.; Berninger, B.; Holt, C. E.; Tessier-Lavigne, M.; Poo, M. *Neuron* **1997**, *19*, 1225−1235.
(14) Wieboldt, R.; Ramesh, D.; Carpenter, B. K.; Hess, G. P. *Biochemistry* **1994**, *33*, 1526−1533.
(15) Warther, D.; Gug, S.; Specht, A.; Bolze, F.; Nicoud, J.-F.; Mourot, A.; Goeldner, M. *Bioorg. Med. Chem.* **2010**, *18*, 7753−7758.
(16) Olofsson, J.; Bridle, H.; Jesorka, A.; Isaksson, I.; Weber, S.; Orwar, O. *Anal. Chem.* **2009**, *81*, 1810−1818.
(17) Atencia, J.; Cooksey, G. A.; Locascio, L. E. *Lab Chip* **2012**, *12*, 309−316.
(18) Tourovskaia, A.; Figueroa-Masot, X.; Folch, A. *Lab Chip* **2005**, *5*, 14−19.
(19) Sims, C. E.; Allbritton, N. L. *Lab Chip* **2007**, *7*, 423−440.
(20) Santillo, M. F.; Arcibal, I. G.; Ewing, A. G. *Lab Chip* **2007**, *7*, 1212−1215.
(21) Takayama, S.; Ostuni, E.; LeDuc, P.; Naruse, K.; Ingber, D. E.; Whitesides, G. M. *Nature* **2001**, *411*, 1016.
(22) Takayama, S.; Ostuni, E.; LeDuc, P.; Naruse, K.; Ingber, D. E.; Whitesides, G. M. *Chem. Biol.* **2003**, *10*, 123−130.
(23) Nielson, R.; Shear, J. B. *Anal. Chem.* **2006**, *78*, 5987−5993.
(24) Moorjani, S.; Nielson, R.; Chang, X. A.; Shear, J. B. *Lab Chip* **2010**, *10*, 2139−2146.
(25) Kawakami, H.; Hiraka, K.; Nagaoka, S.; Suzuki, Y.; Iwaki, M. *J. Artif. Organs* **2004**, *7*, 83−90.
(26) Richardson, R. R.; Miller, J. A.; Reichert, W. M. *Biomaterials* **1993**, *14*, 627−635.
(27) Truskey, G. A.; Yuan, F.; Katz, D. F. *Transport Phenomena in Biological Systems*, 2nd ed.; Pearson/Prentice Hall: Upper Saddle River, NJ, 2004.
(28) Cooksey, G. A.; Sip, C. G.; Folch, A. *Lab Chip* **2009**, *9*, 417−426.
(29) VanDersarl, J. J.; Xu, A. M.; Melosh, N. A. *Lab Chip* **2011**, *11*, 3057−3063.
(30) Taylor, A. M.; Blurton-Jones, M.; Rhee, S. W.; Cribbs, D. H.; Cotman, C. W.; Jeon, N. L. *Nat. Methods* **2005**, *2*, 599−605.
(31) Dertinger, S. K. W.; Chiu, D. T.; Jeon, N. L.; Whitesides, G. M. *Anal. Chem.* **2001**, *73*, 1240−1246.
(32) Kim, T. N.; Campbell, K.; Groisman, A.; Kleinfeld, D.; Schaffer, C. B. *Appl. Phys. Lett.* **2005**, *86*, 201106.
(33) Thangawng, A. L.; Ruoff, R. S.; Swartz, M. A.; Glucksberg, M. R. *Biomed. Microdevices* **2007**, *9*, 587−595.